# EXPERIMENTAL EVALUATION OF COMBUSTOR CONFIGURATION'S IMPACT ON A SWIRL-ASSISTED JET-STABILIZED COMBUSTOR PERFORMANCE

**Saeed Izadi, Jan Zanger, Hannah Seliger-Ost, Peter Kutne, Manfred Aigner**

German Aerospace Center (DLR), Institute of Combustion Technology
Stuttgart, Germany

Email: saeed.izadi@dlr.de

## ABSTRACT

*A major challenge for gas turbine combustor technology is the emission of $NO_x$ and CO. Achieving an optimal premixed, prevaporized, dry low-$NO_x$ condition is a critical issue for liquid fuel combustors. To accomplish this, the relationship between combustor configuration and the performance of a newly developed swirl-assisted jet-stabilized combustor is investigated in an atmospheric combustion facility. The combustor consists of a pressure-swirl fuel atomizer, a prefilmer/mixing channel, an axial moderate swirler (swirl number = 0.6), and a jet nozzle. The jet nozzle allowed for bulk velocities of 50–130 m/s. The influence of each combustor component on combustion performance and fuel evaporation behavior is evaluated independently using optical combustion diagnostics. In addition, the effect of air and liquid fuel temperature on fuel evaporation is characterized. Jet A-1 was injected coaxially into the air stream under both spray and superheated conditions. During the experiments, five critical combustor components were varied to understand their individual effect on fuel vaporization and thus combustion performance. Exhaust gas emissions of $NO_x$, CO and UHC as well as OH* chemiluminescence images were used to evaluate combustor performance. Mie scattering technique was used to analyze the degree of liquid fuel evaporation for different test cases. It was found that the combustion performance indicators CO, height above burner and flame length were well controlled by the degree of fuel evaporation, while NOx emissions showed little change with different combustor configurations. While the main factor influencing the level of $NO_x$ emissions was the adiabatic flame temperature, the quality of fuel evaporation played a minor role. It was found that the operating range of the combustor and the geometric shape of the flame are significantly influenced by the components of the combustor.*

Keywords: Gas turbine, combustor, liquid fuel, Jet A-1, Mie scattering, OH* chemiluminescence, dry low-$NO_x$,

## NOMENCLATURE

| | |
|---|---|
| FLOX | Flameless Oxidation |
| GT | Gas Turbine |
| IBP | Initial Boiling Point |
| LBO | Lean Blowout |
| LDI | Lean Direct Injection |
| LPP | Lean Premix Prevaporize |
| OH* | Hydroxyl Radical, electronically excited |
| PM | Particulate Matter |
| RQL | Rich-Burn Quick-Quench Lean-Burn |
| SCA | Spray Cone Angle |
| $T_{ad}$ | Adiabatic Flame Temperature |
| $T_{air}$ | Air Preheat Temperature |
| $T_{fuel}$ | Fuel Preheat Temperature |
| UHC | Unburned Hydrocarbons |
| $\Delta T$ | Preheat Level of Fuel |

## 1. INTRODUCTION

Reducing the impact of aviation on the environment continues to be a key objective for developers of combustion systems for gas turbines (GT) used in aviation. Increasingly stringent global emission standards have driven the need for cleaner and more sustainable GT combustion systems.

The current aircraft gas turbine engines rely on combustor technologies that aim to maximize efficiency while reducing pollutant emissions. The imposed stringent emission standards by regulatory bodies drive original engine manufacturers to reduce the nitric oxides ($NO_x = NO + NO_2$), carbon monoxide (CO) and particulate matter (PM) emitted by the gas turbines, while maintaining the reliability and efficiency of the engine.

New aircraft engines have improved their emission performance with the adoption of new $NO_x$ limits, as $NO_x$ continues to be a major concern for GT engines. Aircraft $NO_x$ emissions contribute to the greenhouse effect as photochemical changes can lead to an increase of global ozone formation [1], in addition to other human health risks such as respiratory diseases and allergies [2].

The process of burning liquid fuels in GT combustors is inherently more complicated than burning gaseous fuels [3], as there are several additional challenges associated with burning liquid fuels [4]: (A) atomization and vaporization of the liquid fuel, (B) distribution and dispersion of the liquid fuel, (C) spray/mixing channel wall interaction and (D) coking and nozzle blockage

Rapid vaporization of the fuel and subsequent fuel-air mixing prior to the reaction zone is a major challenge in jet-stabilized combustors. To ensure reduced thermal NO, which is the primary $NO_x$ formation pathway under high flame temperature conditions, fuel and air must be mixed under lean conditions for low $NO_x$ operation of the combustor [5]. Some of

the emerging GT combustion concepts are Lean Direct Injection (LDI), Lean Premixed Prevaporized (LPP) and Jet-Stabilized Combustors (FLOX). These concepts promise low-$NO_x$ operation while achieving high combustion efficiencies [6–8]. The combustor system characterized in the current study is principally derived from the jet-stabilized combustor concept.

For a reliable operation of a low-$NO_x$ combustor, flashback, flameout, and other hazardous combustion events must be mitigated. Due to high jet-velocities of the FLOX concept and short fuel-air mixing channel length, its flashback resistance is also improved. However, due to reduced fuel vaporization and limited fuel-air mixing in the mixing channel, the plain jet-stabilized concept has the disadvantage of longer reaction zone, which requires larger liner volume. Adequately designed combustor configuration can significantly influence the combustion performance. The effect of various jet-stabilized combustor configurations is the subject of the current study.

Previous research [9] on the effects of six design parameters of the newly developed swirl-assisted jet-stabilized combustor showed promising results in the $NO_x$ and CO reduction potential of the combustor in both sprayed and superheated fuel injection regimes. In the current work, the mentioned combustor was characterized in depth in term of the effect of its core components on the combustion performance. The combustor uses a moderate swirl (swirl number = 0.6) to enhance the fuel-air mixing and high jet velocities to stabilize the flame. The combustor core components improve the liquid fuel secondary atomization and evaporation prior to the reaction zone.

## 2. LIQUID FUEL COMBUSTOR

The developed combustor investigated in the atmospheric tests is a single-nozzle swirl-assisted jet-stabilized liquid fuel combustor with a concentric fuel injector. In order to evaluate the influence of the main constituents of the Jet A-1 Ref. 3 (see Kathrotia et al. [10] for fuel properties) on the combustion performance, a systematic study was conducted to gain a better understanding of the underlying combustion phenomena.

Sprayed and superheated Jet A-1 ① was injected into the premix channel at different temperatures using a fuel atomizer ④, as shown in Figure 1 *A*. A type-N thermocouple ③ was used to measure the actual fuel temperature 5 mm prior to the fuel atomizer. The premix channel was composed of a prefilmer ⑤ and an axial vane-type swirler ⑥. The prefilmer was a simple DN40 tube with a wall thickness of 0.75 mm and was 60 mm long. The swirler consisted of eight 1 mm straight stainless-steel vanes. Their ends were welded to a 12 mm tube (swirler hub). To prevent fuel and air from passing through, both ends of the hub were blocked. For improved atomization/vaporization of the liquid fuel, the prefilmer and swirler are essential. Before exiting the air nozzle ⑦ into the cylindrical quartz glass combustion chamber ⑧, the preheated air ② is partially mixed with sprayed or superheated fuel.

Figure 1 *B* illustrates a magnified view of the combustor core components. The swirler allowed the formation of a thin fuel film on its vanes' surfaces during liquid fuel spray injection (10). The high air velocity through the swirler vanes led to secondary atomization effect (air-blast effect) (11). In addition, intensified mixing of fuel and air was also made possible by the swirler. By creating a fine film of liquid (12) on its surface, the prefilmer improved the evaporation of the liquid fuel. By increasing the residence time of the fuel on hot surfaces, conductive and convective heat transfer into the fuel is maximized and therefore the prevaporization is enhanced.

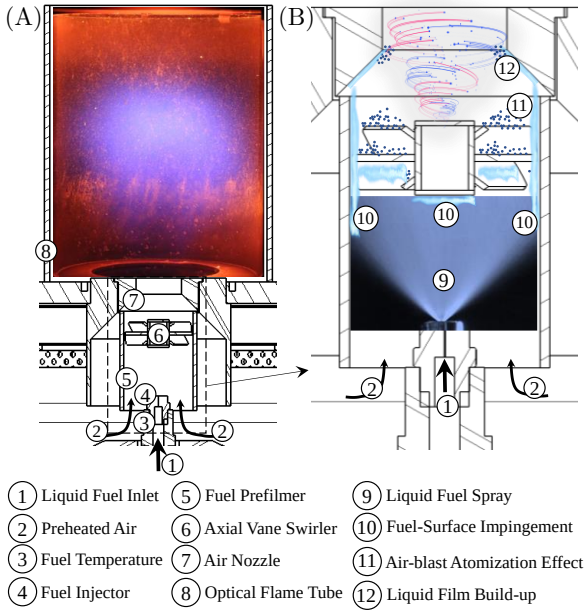


**FIGURE 1: A) SECTIONAL VIEW AND B) COMBUSTOR COMPONENTS MAGNIFICATION. ADAPTED FROM [9]**

In addition, by providing a large surface area, both the prefilmer and the swirler (vanes) prevent most of the fuel from accumulating only on the inner wall of the air nozzle. This provides optimized mixing through swirling and high-velocity jet. Without these components, a build-up of liquid and large droplets at the nozzle exit edge would occur when spraying directly against the inner walls of the air nozzle.

The swirl intensity in a combustor is described by the dimensionless parameter $S_N$. It quantifies the ratio of the axial component of the angular momentum flow to the axial momentum flow [11]. Typically, swirl number less than 0.4 and greater than 0.6 are referred to as weak and strong swirl, respectively. The geometric swirl number is defined as [5]:

$$S_N = \frac{2}{3}\frac{1-(D_{hub}-D_{sw})^3}{1-(D_{hub}-D_{sw})^2}\tan\theta \qquad (2.1)$$

Three main geometry properties are considered: hub diameter ($D_{hub}$ = 12 mm), swirl diameter ($D_{SW}$ = 37 mm) and blade angle ($\theta$ =40 °). Other parameters are the blade thickness (s = 1 mm), the blade height (z = 12.5 mm) and the blade length (c = 17 mm). These parameters lead to the calculation of geometric swirl number $S_N$ = 0.6. This swirl number was chosen because of its efficiency in terms of pressure loss and a lower flame height above the burner than $S_N$ = 0.5. The pressure loss

of $S_N$ = 0.6 (210 Pa) was only 10% higher than that of $S_N$ = 0.5, while the pressure loss of $S_N$ = 0.7 (770 Pa) was 40% higher than that of $S_N$ = 0.5.

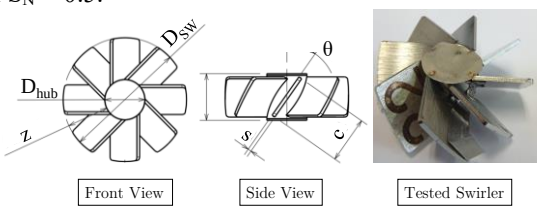


**FIGURE 2: FRONT AND SIDE VIEWS OF THE AXIAL VANE-TYPE SWIRLER**

## 3. CORE COMPONENTS VARIATION

### 3.1 Air Nozzle Diameter Effect

To test the effect of the jet velocity and momentum of the fuel-air mixture, which directly affects the flow field in the flame tube, the air nozzle diameter ($D_{AN}$= 16, 20 and 25.2 mm) was varied. This results in an increase in the dump area ratio from 4.77 to 7.5, which increases the available volume/area for the recirculation zone. The Reynolds number increased from 20,000–26,500 (⌀25.2) to 33,000–43,000 (⌀16). The air nozzle bulk velocity increased from 34.4–45.1 m/s for ⌀25.2 to 85.3–111.5 m/s for ⌀16 mm, resulting in an increased level of turbulence.

### 3.2 Fuel Injector Type Effect

An off-the-shelf simplex pressure-swirl atomizer (Feinzerstäuberdüse TD, manufactured by DIVA Sprühtechnik GmbH, Hamburg, Germany) was used in the experiments.

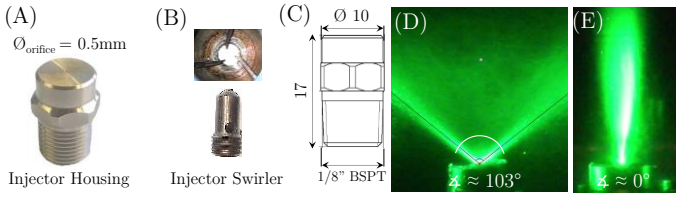


**FIGURE 3: A) FUEL INJECTOR HOUSING; B) INJECTOR SWIRLER, C) INJECTOR DIMENSIONS, SPRAY ANGLE IMAGES OF D) PRESSURE-SWIRL AND E) PLAIN-ORIFICE INJECTOR**

In total, two pressure injector configurations were used during the experiments (hollow cone pressure-swirl and plain-orifice). The DIVA swirler housing was used without its swirler as a plain-orifice injector concept, and the injector swirler was reinstalled for the pressure-swirl injector concept. Figure 3 *A–C* show the DIVA liquid fuel injector housing and its swirler. Figure 3 *D–E* show, at a Jet A-1 mass flow rate of 0.52 g/s, Mie scattering images with spray angles of 103° for the pressure-swirl and ≈ 0° for the plain-orifice injector. A pressure drop of 4.5 bar was required for the swirl injector and 2.5 bar for the plain-orifice injector for this mass flow rate at fuel temperature $T_{fuel}$ = 155°C.

### 3.3 Combustor Core Components Effect

Understanding the influence of each of the combustor core components on the flame shape, the operating range of the combustor, the fuel evaporation, and the quality of the exhaust gas emissions is essential in developing the combustor system. For this purpose, as shown in Figure 4, detailed experiments are performed in the absence and presence of some of the combustor core components.

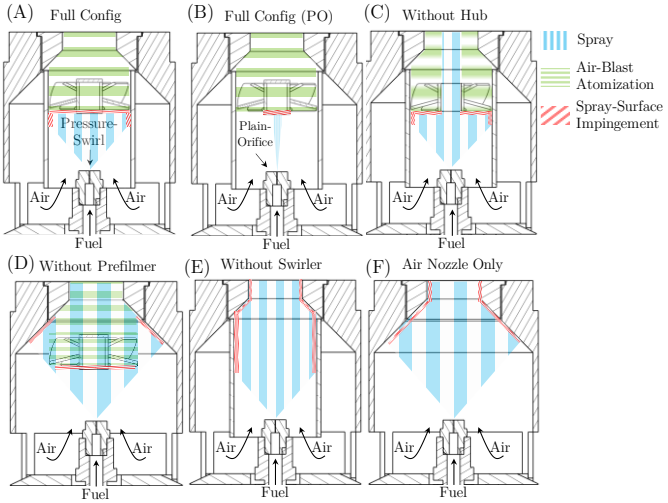


**FIGURE 4: ILLUSTRATION OF THE SWIRL-ASSISTED JET-STABILIZED COMBUSTOR CORE COMPONENTS VARIATION TESTS**

The spray path of the liquid fuel is shown in Figure 4 in as vertical lines. The areas where the fuel is being atomized due to the secondary atomization (air-blast effect) are shown as horizontal lines. The area where the fuel droplets impinge is colored as diagonal lines. The swirl-assisted jet-stabilized combustor is used as the reference case, where all of the components are installed. This is referred to as the Full Config configuration of the combustor, where the fuel injector is a pressure-swirl type (see Figure 4 *A*). For the configuration with the plain-orifice injector, the Full Config was used to solely observe the atomizer spray characteristics effects (see Figure 4 *B*).

In the next step, the swirler hub was removed from Full Config. This allowed unobstructed fuel and air flow through the center of the swirler in both spray and superheated conditions. This is referred to as a w/o Hub combustor configuration (see Figure 4 *C*). To isolate the swirler's influence on combustion performance, the next combustor modification was to move the swirler hub back and remove the prefilmer channel. This is designated as w/o Prefilmer configuration (see Figure 4 *D*). The prefilmer is reinstalled and the axial swirler is removed in the next configuration. This is done to study how the swirler affects flame characteristics and fuel vaporization. This is referred to as the w/o Swirler configuration (see Figure 4 *E*). The final step was similar to the unmodified single-jet stabilized combustor that had been tested in previous studies [12–14]. This is referred the Air Nozzle Only combustor configuration (see Figure 4 *F*).

## 4. MEASUREMENT INSTRUMENTATION

### 4.1 Mie Scattering

Scattering refers to the deflection of electromagnetic radiation from its original path when a photon of light encounters an irregularity in the medium through which it is travelling. In this case, the medium is air and irregularities are the fuel droplets. The amount of scattering is determined by the wavelength of the light and the size of the particles in the medium. If the particle size is equal to or greater than the wavelength of the light, Mie scattering occurs. [15]

In order to observe the individual fuel evaporation behavior and spray shape characteristics, two different experimental setups (reactive and non-reactive) were used in this work. In the reactive experiments, a laser sheet with a thickness of 1 mm and a height of 17 mm was used to illuminate fuel droplets. A schematic of the Mie scattering setup is shown in Figure 5 *A*. A high-speed camera (LaVision HighSpeedStar 6) with a Nikon 50 mm f1.8 lens made the spray contours visible by Mie scattering. Only the laser light reached the camera sensor through an interference filter with a center wavelength of 532 nm. A collimated diode pumped solid state (DPSS) continuous wave laser (Thorlabs CPS532) was used to illuminate the observed spray. The laser wavelength was 532 nm and the laser power was 4.5 mW.

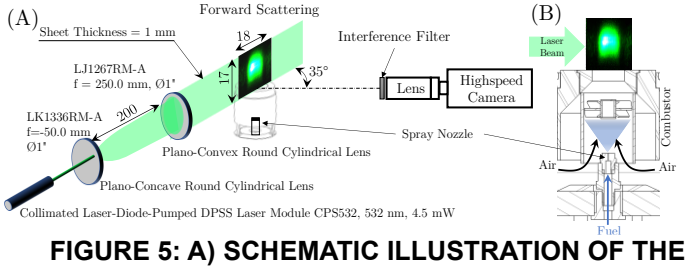


**FIGURE 5: A) SCHEMATIC ILLUSTRATION OF THE MIE SCATTERING MEASUREMENTS FOR THE REACTIVE TESTS, B) FUEL NOZZLE POSITION**

For the reactive tests, the Mie scattering intensities were recorded at a repetition rate of 1 kHz and an exposure time of 83 µs for 1000 instantaneous images for each image sequence. As shown in Figure 5 *B*, the injector nozzle was in its original position at the combustor inlet.

The non-reactive tests detailed in Section 6.1 aimed at analyzing the behavior of the liquid fuel spray immediately after injection and vaporization at different fuel temperatures. Unlike the reactive test, where the injector was positioned inside the combustor (see 4.1 *B*), for the non-reactive test, the injector lance was extended axially. Therefore, while moving the injector through the air nozzle up to the flame tube inlet, the Mie scattering of the droplets was measured. This way, the entire process of fuel atomization could be observed immediately after the fuel injection without the effect of the combustor configuration in terms of enhanced fuel evaporation and secondary atomization. In the non-reactive Mie scattering measurements, the liquid spray was illuminated by a 1 mm thick and 25 mm high laser light sheet. As in the reactive tests, the same high-speed camera was used but at a repetition rate of 50 kHz and an exposure time of 19.33 µs. However, to extend the axial length of the laser sheet, a plano-convex cylindrical lens of H30 x L60 $mm^2$ was used. Thus, the variation of the axial penetration of the liquid phase along the combustor axes could be observed. All pixel intensities less than 10 counts were set to zero to remove any small laser light reflections on the combustion chamber quartz glass for both reactive and non-reactive tests. The images were then time-averaged and normalized to their maximum intensity to allow comparison of evaporation behavior.

### 4.2 OH* Chemiluminescence

The chemiluminescence signal of the electronically excited OH* radical was used to analyze the geometric characteristics of the combustion zone. OH* is a good indicator of the location of the heat release zone because it is formed predominantly in the reaction zone and has a very short lifetime. [16,17]

To analyze the geometric characteristics of the flame the OH*-chemiluminescence (OH*-CL) intensity was recorded for all operating points using a CCD camera combined with an intensifier (LAVISION: Intensified Relay Optics), a CERCO 100 mm UV lens F/2.8 and a UV interference filter (312 ± 15 nm). All OH*-CL images were acquired with a constant gain of 65%. The gate time was 400 µs. By processing 200 single instantaneous images at a repetition rate of 26 Hz, the signal intensity of each flame was analyzed.

A routine developed by Zanger [18] was used to calculate the flame length (FL) and height above burner (HAB), from the time-averaged OH*-CL images. Refer to Bower et al. [19] for detailed description of the routine. For OH*-CL measurements, the camera field of view of the OH*-CL is centered in the axial direction of the combustor. This allowed the observation of the whole optically accessible flame tube. With an image resolution of 5 pixels per mm, the camera system was placed approximately 1500 mm from the combustor.

### 4.3 Exhaust Gas Emission

A commercially available emission analyzer, ABB: Advanced Optima Process Gas Analyzer AO2000, was used to measure the exhaust gas concentrations for all operating points. All analyzer sensors were calibrated prior to each measurement day. At a single point concentric with the flame tube, 566 mm from the burner front plate, a gas composition sampling probe was installed in the exhaust gas section.

The use of a suction probe with a coaxial air cooling system sufficiently quenched chemical reactions as well as surface reactions due to hot probe walls. This reduces surface reactions that could distort the gas composition by preventing excessive temperatures on the outer wall of the probe. The cooler probe wall prevents surface reactions on the outer wall of the probe. This makes it possible to have defined measuring conditions for all different operating points of the combustor when exhaust gas measurements are made.

A total of 180 measurements were taken over 3 minutes (at 1 Hz) for each operating point. Recording the composition of the emitted gases and the OH* images was started after a steady state was reached, i.e. the UHC, CO and $NO_x$ emissions did not change significantly over time. The emission concentrations

were normalized to dry conditions at a residual oxygen content of 15 vol% in parts per million by volume dry (ppmvd). The UHC emissions remained at a constant level of 0.16-0.3 ppm over the entire temperature range of the flames. These values are below ABB's UHC measurement accuracy of ±0.37 ppm. Therefore, the possible influence of the characterized factors on the UHC behavior is not analyzed and will be neglected.

## 5. EXPERIMENTAL DESIGN SPACE

Jet A-1 with an initial boiling point of $T_{IBP}$ = 141.1°C, a volume average boiling point of $T_{VABP}$ = 206.9°C and a final boiling point of $T_{FBP}$ = 270.3 °C was used throughout the atmospheric experiments. As listed in Table 1, the thermal power $P_{th}$ = 22.5 kW (0.52 g/s Jet A-1) of the combustor was kept constant. The adiabatic flame temperature was varied from $T_{ad}$ = 1750–2050 K mainly by increasing the air mass flow rate. The air preheat temperature was varied between $T_{air}$ = 155–255°C. For the entire combustor configuration variation tests described in Section 3.3, the air nozzle was kept at constant diameter of $D_{AN}$ =16 mm. The diameter of the flame tube was kept constant at $D_{FT}$=120 mm. Swirl number is also held constant at $S_N$ = 0.6 if installed.

**TABLE 1: EXPERIMENTAL PARAMETERS**

| Parameter | Unit | Low Level | Baseline | High Level |
|---|---|---|---|---|
| $T_{ad}$ | [K] | 1750 | 1900 | 2050 |
| $T_{air}$ | [°C] | 155 | 205 | 255 |
| ΔT | [K] | -100 & -50 | 0 | 50 |
| $P_{th}$ | [$kW_{th}$] | | 22.5 | |
| $D_{FT}$ | [mm] | | 120 | |
| $D_{AN}$ | [mm] | | 16 | |
| $S_N$ | [-] | | 0.6 | |

Since the superheated injection concept was used to atomize and then vaporize the liquid fuel, the level of preheat ΔT (see Equation 4.1) was used to evaluate the relative fuel temperature $T_{fuel}$ from its saturation temperature $T_{sat}$ ($p_\infty$), which varies at different back pressures $p_\infty$. For a fuel temperature variation of $T_{fuel}$ = 105–255°C, the level of preheat amounted to ΔT = - 100–50 K, considering Jet A-1 $T_{sat}$ (p = 1 atm) ≈ 205°C [20].

$$\Delta T = T_{fuel} - T_{sat}\,(p_\infty) \qquad (4.1)$$

Multivariate analysis was used to analyze the data obtained in the current work as a part of the Design of Experiments (DOE) methodology. For further insight into the subject matter, refer to previous work [9].

## 6. RESULTS AND DISCUSSIONS

### 6.1 Fuel Injector Type Effect

In this section, the effect of atomization quality on flame combustion performance is investigated by characterizing two fuel injectors based on pressure-swirl and plain-orifice, as shown in Figure 3 In a combustion process, the combustion performance can be significantly affected by the quality of the fuel spray.

As described in Section 4.1, in order to characterize the combustion, it was necessary to determine the spray shape and angle, the radial and axial penetration depth of the fuel and the fuel evaporation degree. For this purpose, a Mie scattering measurement (W20 x H25 $mm^2$) was performed for a wide range of fuel temperatures (150–300°C) at atmospheric backpressure for both injector types. Figure 6 shows Mie images of a selected range of $T_{fuel}$ = 190–280°C. For both injector types, the atomization behavior of the fuel remained constant from 150–200°C. The Mie scattering measurement was performed in a non-reactive setup without the flame effect.

For the pressure-swirl injector, the expected injection regime of mechanical fuel break-up as a spray is dominant from room temperature up to 200–210°C. This is the point at which the transition to the superheated regime takes place. Thermal fuel breakup essentially begins at about 220°C at atmospheric backpressure. The spray cone angle (SCA) appears to decrease steadily from approximately 100° at room temperature to 80°, 70°, and 30° at 150°C, 200°C, and 250°C, respectively. After the transition to the superheated regime, the hollow cone gradually changes to a solid spray cone with increasing fuel temperature. As the superheated and pressurized fuel expands into the atmospheric pressure, fuel vapor bubbles are formed within the liquid bulk. This leads to a rapid formation of larger bubbles near the injector outlet. The bubbles grow and then collide with each other, where a fine plume is formed. The absence of the hollow spray cone reduces the radial penetration of the fuel and can cause a significant deterioration in the mixing of fuel and air. For both injectors, the transition of the liquid fuel to the gaseous phase can be well observed, where the Mie scattering signal decreases with increasing fuel temperature.

The gradual decreasing axial penetration of the liquid phase is clearly seen. This is an indication of an increase in fuel evaporation as a result of increasing ΔT. Liquid fuel expands and accelerates downstream of the flow as it evaporates. This results in a narrow stream of vaporized fuel entering the reaction zone unless slowed by a baffle. Localized fuel-rich pockets can result from this unrestricted fuel flow. In addition, the inhomogeneous mixing of fuel and air can reduce the flame stability range, resulting in higher flame temperatures, which can facilitate increased $NO_x$ formation. The bottom row in Figure 6 shows the Mie signals of the fuel with the plain orifice injector. The required injector pressure loss of 2–3 bar in the temperature range of 150 to 240°C was not sufficient to induce a significant mechanical breakup of the liquid fuel at the nozzle exit. The injector orifice diameter was relatively large at 500 µm and the fuel mass flow was relatively small at 0.52 g/s. Therefore, a jet of liquid fuel dominated over most of the fuel temperature range up to 240°C. Note that, due to the eccentricity of the liquid fuel jet from the laser sheet as a result of a skewed fuel injection, some of the instantaneous images show interrupted Mie signals. The bottom of the spray is visible because the laser sheet is centered in the injector orifice. The top of the spray is also visible as the fuel jet widens due to spray buildup. In some cases, the center of the spray is not visible due to a skewed fuel jet.

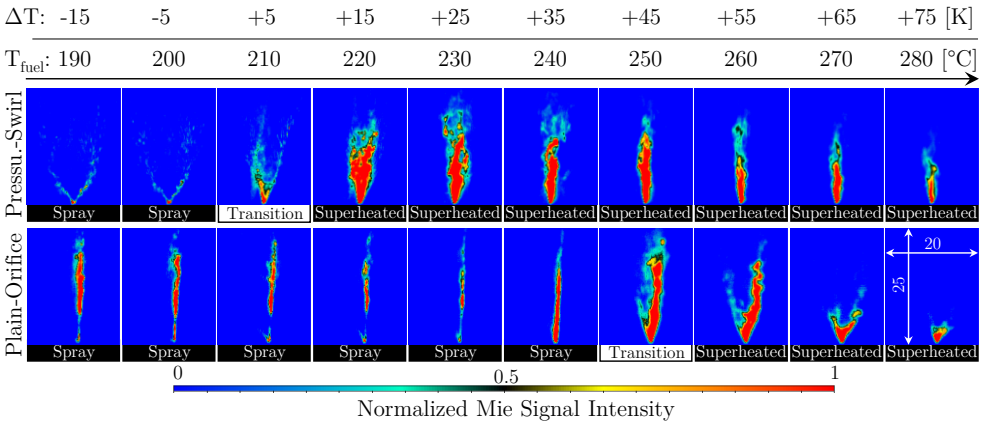


**FIGURE 6: INSTANTANEOUS MIE IMAGES FOR TWO FUEL INJECTORS AT DIFFERENT TEMPERATURES**

For the plain-orifice, the transition point is measured at 250°C, the point at which the fuel jet becomes a plume. This higher transition temperature than pressure-swirl injector could be due to the lack of swirling motion of the fuel in the injector and the resulting sprayed sheet. Similar to the pressure-swirl injector, the superheated regime, characterized by a highly turbulent fuel plume, covers more of the laser sheet area and emits more signal to the camera. The superheated fuel of plain-orifice undergoes faster thermal breakup into fine droplets that evaporate at higher rates than the pressure-swirl injector. Compared to the pressure-swirl injector, the axial penetration depth of the fuel plume at 280°C appears to be much shorter due to faster evaporation.

For both injector types, the Jet A-1 spray behavior with increasing fuel temperature was demonstrated in the non-reactive tests discussed earlier. For the reactive tests, the injector was returned to its original position in the combustion chamber (see Figure 5 *B*).

The $NO_x$ (black curves and left y-axis) and CO (red curves and right y-axis) emissions as a function of the adiabatic flame temperature $T_{ad}$ = 1730 to 2350 K and the level of preheat ΔT = - 50 and 0 K for the pressure-swirl and plain-orifice injectors are shown in Figure 7 .

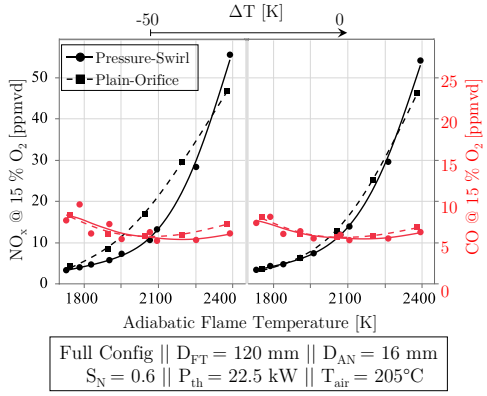


**FIGURE 7: EXHAUST GAS EMISSIONS OF THE FUEL INJECTORS; A) $NO_x$ AND CO**

Due to partial evaporation of fuel in the plain orifice injector, it was not possible to operate the plain-orifice at ΔT = +50 K because the fuel pressure drop was much lower at 2–3 bar compared to 13–15 bar for the pressure-swirl injector. The saturation temperature of the pressurized fuel was lower due to the lower pressure drop of the injector. This resulted in nozzle choking due to gaseous fuel ejected through the 500 µm orifice at higher fuel temperatures (> 220°C). However, in the non-reactive tests, a higher injector pressure loss was achieved due to partial nozzle orifice blockage from coking, which prevented fuel vaporization in the nozzle.

The general progression of $NO_x$ values with increasing $T_{ad}$ appears similar for both injector types at both ΔT, but the $NO_x$ trend of the plain-orifice at ΔT = -50 K appears to increase more rapidly. Under fuel-richer conditions, and therefore higher flame temperatures, the rate of NO formation will increase as a result of the Zeldovich mechanism. The $NO_x$ values for both injector types differ negligibly by only 1 ppm at $T_{ad}$ = 1730 K and ΔT = -50 K, where the fuel-air mixture is leanest and the spray is mostly liquid. This is because the velocity in the prefilmer channel is maximum at 17 m/s at the highest air equivalent ratio, as the airflow is varied and the fuel flow/thermal power is kept constant. This results in an increased air-blast fuel atomization effect on the leading and trailing edges of the swirler. As an effect, the quality of the fuel spray prior to the reaction zone is similar for both injector operations.

At $T_{ad}$ = 2065 K, with $NO_x$ = 17 ppm for the plain-orifice, the $NO_x$ difference increases to 6.5 ppm. As the velocity in the prefilmer channel decreases to 13.1 m/s, the impingement of the fuel jet on the swirler hub and the subsequent secondary atomization by the air-blast effect become insufficient to form comparable fuel droplets. Thus, fuel and air mixedness decreases as larger fuel droplets enter the reaction zone. The pressure-swirl $NO_x$ level exceeds that of the plain-orifice by a difference of 9 ppm, with the pressure-swirl $NO_x$ level at 55.5 ppm, as the flame temperature reaches its highest value at $T_{ad}$ = 2350 K. It is because the reaction zone of the pressure-swirl injector is much more concentrated due to improved fuel atomization, as shown in Figure 8 *A*. Plain-orifice injector reaction zones appear to be more dispersed and less concentrated.

$NO_x$ levels appear to follow a similar trend in rate and magnitude for both injector types at ΔT = 0 K. This is due to the

fact that at $\Delta T = 0$ K ($T_{fuel} = 205°C$), the fuel droplet size of the plain-orifice injector decreases at higher fuel temperatures and becomes comparable to that of the pressure-swirl injector. Increasing fuel temperature not only causes faster fuel evaporation, but also reduces viscosity, improving spray quality. In spite of the inferior atomization quality of the plain-orifice injector, the $NO_x$ values of the flames are largely comparable for both types of injectors, mainly due to the additional internal parts of the combustor (prefilmer and swirler). If the straight fuel jet would not hit the swirler hub, the difference would certainly be more pronounced. However, for this type of combustor, this also means that the quality of the primary atomization is not the determining factor.

As shown in Figure 7, CO emissions for both injector types remain constant at all $\Delta T$ levels and throughout the $T_{ad}$ range, with a maximum value of 9.5 ppm and a minimum value of 6.1 ppm. Sufficient residence time of the species in the flame tube allows for oxidation of most of the CO into $CO_2$.

Figure 8 *A* shows an OH* image matrix (W120 x H160 $mm^2$) of the reaction zone for the plain-orifice (top row) and pressure-swirl injectors (bottom row) for a range of $\Delta T$ = -50 to 50 K. Among other parameters (see figure legend), $T_{ad}$ is kept constant at 2350 K. For each of the injector types, an increase in $\Delta T$ results only in a slight change in flame shape and position, while the emitted OH* emission is significantly different between the two injectors due to the different compactness of the reaction zone. The smaller fuel droplets produced by pressure-swirl evaporate faster, resulting in a more concentrated and compact reaction zone. This may explain why at $T_{ad}$ = 2350 K the pressure-swirl flame had higher $NO_x$ levels.

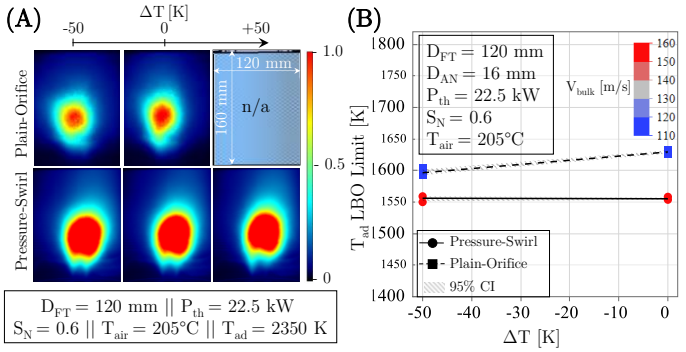


**FIGURE 8: A) OH* IMAGES AND B) LBO LIMITS FOR DIFFERENT ΔT AND FUEL INJECTORS**

Each LBO test was repeated three times in order to gain statistical confidence in the results. The air mass flow rate was manually increased at a rate of 0.02 gram per second ($\Delta T_{ad}/\Delta t$ = 2 K/s).

The LBO limits for both injector types are shown in the combustor operating range in Figure 8 *B*. Overall, the pressure-swirl injector flames had a constant LBO range over the tested $\Delta T$ levels at ≈ 1550 K. However, the $T_{ad}$ LBO limit increased from 1600 K to 1632 K for the plain-orifice injector as $\Delta T$ increased from -50 to 0 K. The 50 K difference in the LBO limits for the two injector types at $\Delta T$ = -50 K is due to the larger droplets formed by the plain-orifice injector and the consequent longer droplet evaporation time. This results in a degraded fuel-air mixing quality. The reduced fuel-air mixing at near-superheated conditions explains the small increase of 32 K in the LBO limit of the plain-orifice flame.

### 6.2 Fuel Evaporation Characterization

A detailed study of the effect of fuel and air temperatures on the fuel evaporation and the subsequent effect on the size and position of the flame is given in this section. For these reactive tests, the pressure-swirl fuel atomizer was used.

A matrix of time-averaged images of Mie signals (W18 x H17 $mm^2$) recorded during the reactive tests is shown in Figure 9 for an air preheat temperature $T_{air}$ range of 155 to 255°C (rows) and a fuel preheat level $\Delta T$ range of -100 to 50 K (columns). These signal intensities are a qualitative description of the size and density of the fuel droplets in the vicinity of the head of the combustor.

Because the fuel nozzle sprays directly against the inner walls of the prefilmer and the axial swirler vane surfaces (see Figure 1 *B*), the fuel appears to enter the flame tube circumferentially from the air nozzle lip. In addition, the fuel is prevented from exiting near the air nozzle axis by the swirler hub and the swirling motion of the mixture. The signal-to-noise ratio of the reactive experiments shown in Figure 9 was measured to be half that of the non-reactive experiments shown in Figure 6, mainly due to smaller fuel droplets emerging from the combustor nozzle, resulting in a reduced Mie scattering signal detected by the camera sensor in the reactive experiments.

Due to the bell-shaped laser energy distribution, it appears that only the middle ≈ 10 mm (area between the beginning and end of the laser sheet) of the fuel spray is visible to the camera. This is despite the fact that 4 mm of the upper and lower sides of the laser sheet were mechanically trimmed (laser sheet height reduction from 25 to 17 mm). This was done to allow the more intense signal to pass through the measurement area.

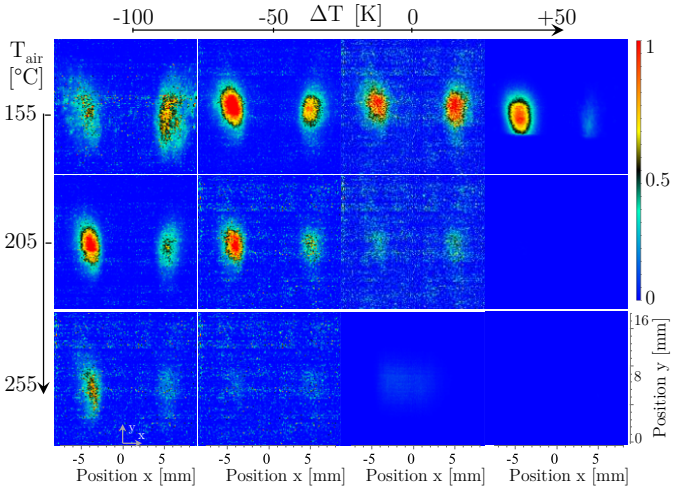


**FIGURE 9: TIME-AVERAGED MIE SCATTERING IMAGES OF JET A-1 IN THE REACTIVE TEST**

The effect of the air temperature on fuel evaporation degree can be seen by the decrease in intensity of the fuel Mie signal as the $T_{air}$ increases from 155 to 255°C. Looking at the first image-column on the left, it appears that the signal intensities for all three $T_{air}$ levels are asymmetric. This asymmetry varies from the upper plot to the plot in the middle, where more liquid is detected on the left-hand side than on the right-hand side. An asymmetric spray formation of the fuel nozzle is one explanation for this behavior. Due to absorption and scattering of laser energy by the fuel droplets on the left side, a reduced signal is detected on the right side of the image.

Most of the fuel was in the liquid phase at ΔT = -100 K and $T_{air}$ = 155°C. This is due to the fact that ΔT is below the Jet A-1 initial boiling point (IBP) of 141.1°C. The first row shows an increase in ΔT = -100 to 50 K at $T_{air}$ = 155°C. A significant change occurs when ΔT reaches +50 K, where fuel almost disappears from the right side of the image. Fuel in the liquid phase can be observed despite the superheated injection of the Jet A-1 and its subsequent evaporation (see Section 6.1 and Figure 6). Due to the relatively low $T_{air}$ = 155°C, condensation of the superheated injected fuel at ΔT = +50 K should have occurred on the inner surfaces of the combustor and in the flowing air. The lowest air temperature required for complete fuel vaporization without fuel condensation is the temperature combination of ΔT = +50 K and $T_{air}$ = 205°C.

Figure 10 shows a corresponding matrix of OH*-images for the tested operating conditions shown in Figure 9. It appears that the OH* emission intensity of the reaction zone increases with increasing $T_{air}$ from 155 to 255°C for all ΔT levels. The reaction zone symmetry disappears with increasing ΔT from 0 to +50 K. The lift-off height also increases in this ΔT range. This indicates a different fuel-air mixture as a result of fuel superheated injection.

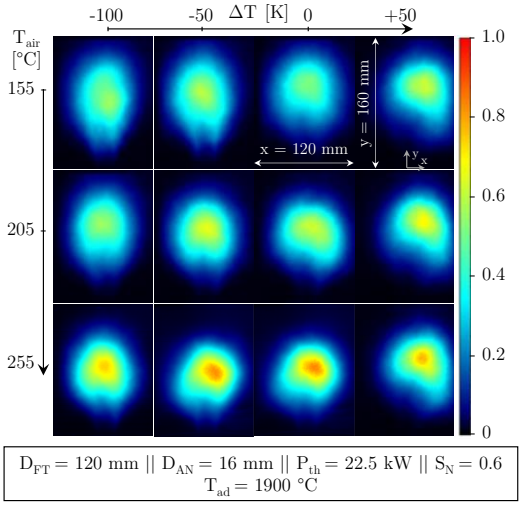


**FIGURE 10: FLAME OH* IMAGES: ΔT VS. $T_{AIR}$**

The resulting HAB values are shown in Figure 11 A. At $T_{air}$ = 155°C, an increase in ΔT from -100 to +50 K results in a large increase in HAB from 56.5 to 75.2 mm. Meanwhile, at ΔT = - 100 K, increasing $T_{air}$ from 155 to 255°C results in a relatively small increase in HAB (56.5–62 mm). The strong difference in ΔT and $T_{air}$ effects on HAB levels demonstrates that an increase in $T_{fuel}$ (ΔT) has a more dominant effect on fuel evaporation. This is due to the reduced radial penetration of the fuel into the coaxial air flow and the simultaneous rapid axial expansion of the fuel, which reduces the reactivity of the bulk mixture.

The flame length values shown in Figure 11 *B* show that as ΔT increases from -100 K to +50 K, FL levels decrease moderately from 61.5 to 44 mm. However, for an increase of $T_{air}$ from 155 to 255°C, FL values decrease slightly from 61.5 to 54 mm. It appears that fuel temperature has a more significant effect on reducing flame length than air temperature. While an increase in ΔT has an effect on fuel evaporation, an increase in $T_{air}$ from 155°C to 255°C results in an increase in both fuel evaporation and bulk velocity of 15 m/s, which may counteract the effect of fuel evaporation in reducing the flame length.

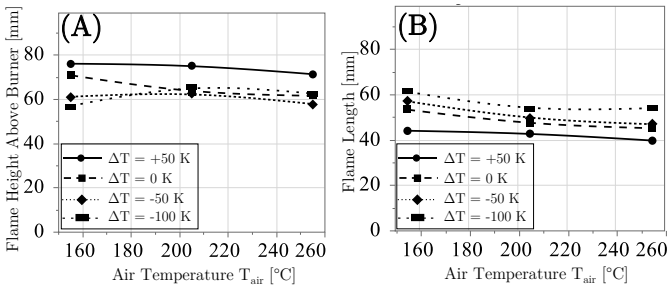


**FIGURE 11: (A) HAB, (B) FL AT VARIOUS ΔT, $T_{AIR}$**

### 6.3 Air Nozzle Diameter Effect

As described in Section 3.1, for the tested air nozzle diameters $D_{AN}$ = 16, 20 and 25.2 mm, the combustor dump area ratio varied from 7.5, 6 and 4.77 for a constant flame tube diameter $D_{FT}$ = 120 mm. The effect of the reduction in $D_{AN}$ and the consequent increase in bulk velocity on $NO_x$ is shown in Figure 12 *A*. The lowest $NO_x$ throughout the $T_{ad}$ range are consistently observed at the lowest $D_{AN}$ = 16 mm. The reduction in $D_{AN}$ results in improved fuel-air mixing with increased air dispersion at the nozzle exit for a constant mass flow rate. Increasing the velocity leads to increased Reynolds number and thus increased turbulence. Improved mixing is achieved by increasing recirculation rate, resulting in increased fresh and exhaust entrainment in the shear layer. Up to a certain limit, it can also positively affect the formation, size and intensity of the recirculation zone within the flame tube. This is critical to stabilizing the flame and reducing emissions.

For $T_{ad} \leq 1900$ K, the variation appears smallest with $NO_x$ values of 4.2, 6.1 and 8.2 ppm for $D_{AN}$ = 16, 20 and 25 mm. The $NO_x$ variation is highest at the highest adiabatic flame temperature with 5.5, 11.8 and 17 ppm for $D_{AN}$ = 16, 20 and 25.2 mm, respectively. Higher velocities increase the degree of turbulence and change the flow pattern within the flame tube. The Reynolds number increases from 21,900 to 34,500 as the air nozzle diameter decreases from 25.5 to 16 mm at $T_{ad}$ = 2050 K. This leads to an improvement in the hot recirculation zone and rates. Lower residence time as a result of increased velocity can

reduce NO formation by affecting the amount of time products spend in the recirculation zone.

The effect of $D_{AN}$ variation on CO emissions is shown in Figure 12 *A*. The slight increase in CO at fuel-lean conditions is clearly seen. A possible explanation is the quenching effects near the LBO limits, in addition to the lower flame temperature and shorter residence time. This may also be caused by insufficient residence time in the hot zone to allow the CO to oxidize to $CO_2$. The absolute differences in CO emissions for $D_{AN} = 20$ and 25.2 mm over the entire $T_{ad}$ range are in the range of 0.5–2.5 ppm. This is a marginal difference. The measured CO was 8.3 ppm for $D_{AN} = 16$ mm and 10.7 ppm for $D_{AN} = 20$ and 25.2 mm at $T_{ad} = 1900$ K. It appears that the residence time for all three nozzle diameters provided the time required for most of the CO to oxidize to $CO_2$ in the flame tube. For $D_{AN} = 16$ mm, due to higher momentum at lower $T_{ad}$ (1638 K), the exhaust gas exits the reaction zone faster, leading to a slight increase in CO emissions. For the same combustor and operating parameters, the total combustor pressure loss increased from 1.05% to 3.75% at $T_{ad} = 1900$ K by reducing the air nozzle diameter from $D_{AN} = 25.2$ to 16 mm.

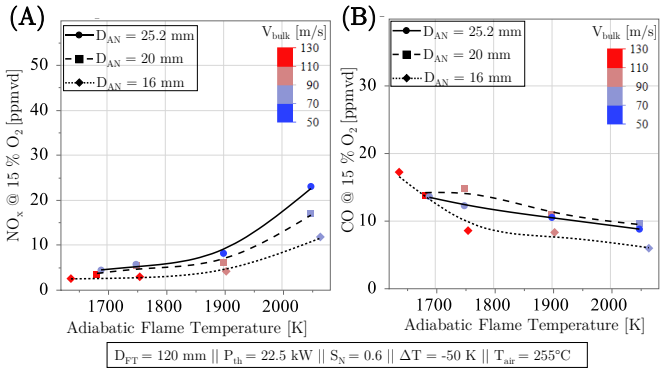


**FIGURE 12: (A) NOX AND (B) CO PLOTS OF VARIOUS AIR NOZZLE DIAMETERS**

### 6.4 Combustor Core Components Effect

Understanding how each combustor core component affects flame shape, operating range, fuel evaporation, and exhaust gas quality is essential for further enhancing the combustor's performance. To do so, additional detailed experiments are performed in the absence and presence of some of the core elements, as shown in Figure 4. To investigate the effect of fuel and air as a function of combustor configuration, Mie scattering measurements were performed as shown in Figure 5 *A*. The fuel injector was the pressure-swirl type and positioned at its original location (see Figure 5 *B*). Each tested configuration produced different degrees of fuel evaporation and droplet patterns, as shown in Figure 13.

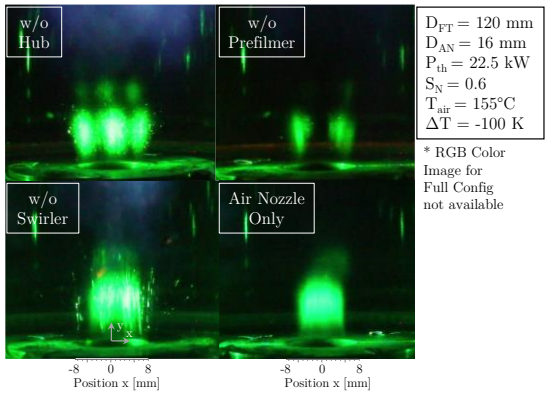


**FIGURE 13: INSTANTANEOUS JET A-1 MIE SCATTERING IMAGES FOR FOUR CONFIGURATIONS**

Time-averaged Mie signal images (W18 x H17 $mm^2$) using a high-speed camera are shown in Figure 14, where $T_{air}$ is varied from 155 to 255°C (rows) for all five combustor configurations (columns) at a constant $\Delta T = -100$ K and $T_{ad} = 2050$ K. The air and fuel mass flow rates are also kept constant. For all configurations, as the air temperature increases, the Mie signals seem to be decreasing, which is an indication of increasing fuel evaporation and decreasing fuel droplet size. For each configuration, the reduction in Mie signals appears to be different. For example, due to the secondary fuel atomization caused by the swirler vanes and the enhanced fuel-air mixing, the configurations with the swirler (Full Config (A), w/o Hub (C), and w/o Prefilmer (D)) show the greatest reduction in Mie signals. As $T_{air}$ exceeds Jet A-1 saturation temperature at $T_{sat}$ (p = 1 atm) ≈ 205°C, Mie signal intensities decrease more rapidly at $T_{air} = 255$°C. At this air temperature, the Full Config, w/o Hub, and w/o Prefilmer configurations show minimal Mie signals as opposed to the w/o Swirler (E) and Air Nozzle Only (F) configurations. This reflects the substantial effect of the prefilmer and swirler on fuel evaporation.

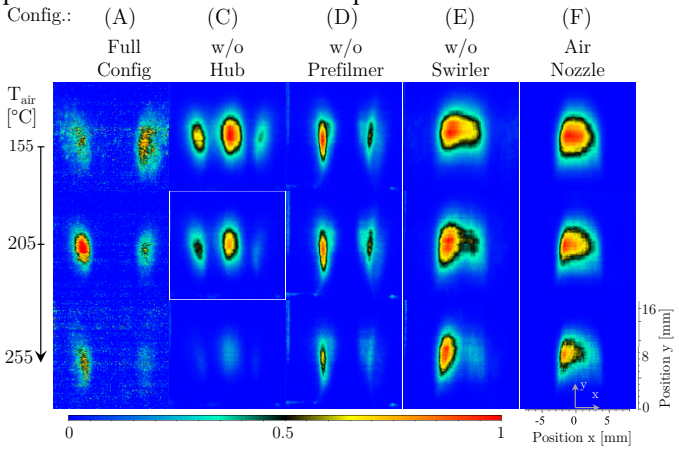


**FIGURE 14: TIME-AVERAGED MIE IMAGES FOR CONFIGURATION AND $T_{AIR}$ VARIATION AT $T_{AD}$ = 2050 K AND $\Delta T$ = -100 K**

By comparing the two image-columns on the left, the effect of the swirler hub can be seen. It appears that unblocked fuel droplets exit the combustor near its axis as well as through the

swirling vanes. This leads to decreased fuel evaporation rate and extended flame lengths. The middle column (D) shows the effect of the prefilmer in improving fuel atomization. Compared to the Full Config (A) (including the prefilmer), an increasing amount of fuel is being discharged in the axial direction from the combustor nozzle. The wider spray observed with the full configuration can be an indication of finer and better mixing of the fuel droplets with the air. The installation of the prefilmer reduced the cross-sectional area by a factor of 3.77. The fuel-air velocity increased by the same factor. The result was a reduction in fuel droplet residence time in the mixing channel. However, the increase in velocity resulted in improved secondary fuel atomization by increasing the air-blast effect on the leading and trailing edges of the swirler blades.

By slowing the axial flow of the fuel-air mixture, the swirler increases the residence time of the fuel droplets and their mixing with the air. This increase in residence time may be a result of the more complex nature of the flow. This results in increased evaporation compared to the w/o Swirler (E) and Air Nozzle Only (F) configurations. The other combustor configurations show different patterns of exiting liquid fuel except for the w/o Swirler and Air Nozzle Only configurations where the Mie signal intensities are largely similar. At $T_{air}$ = 255°C, due to the reduced velocity of the fuel-air mixture in the mixing channel in the Air Nozzle Only configuration, the residence time of the fuel droplets is longer than in the w/o Swirler (E) configuration. The result is an increase in fuel droplet vaporization.

Figure 15 shows the OH* image matrix for the described combustor configurations at three $T_{ad}$ levels of 1750 K, 1900 K, and 2050 K at $\Delta T$ = 0 K. Because of the significantly reduced operating range of the w/o Swirler and Air Nozzle Only configurations, only one lean flame condition could be operated stably at $T_{ad}$ = 2350 K. No emission measurement was performed for these two configurations due to the presence of unvaporized fuel droplets in the flame tube and downstream of the reaction zone. These unevaporated fuel droplets would have had an adverse effect on the ABB gas analyzer during their passage through the probe.

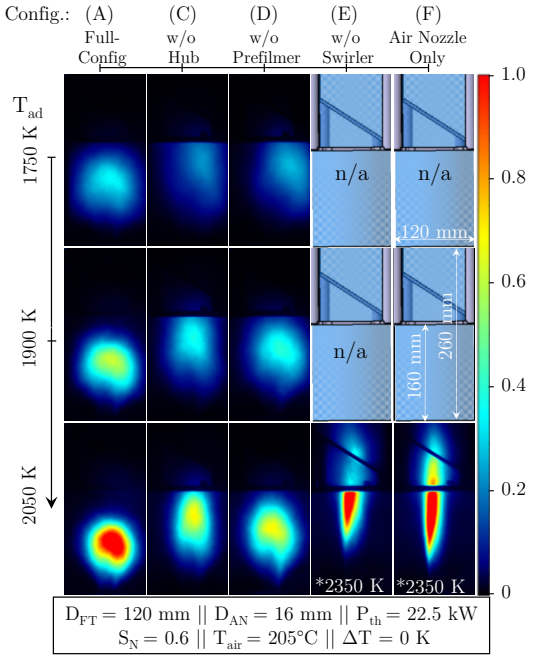


**FIGURE 15: OH* IMAGES FOR ALL FIVE COMBUSTOR CONFIGURATIONS**

At any $T_{ad}$ level, the full configuration has the most compact heat release zone of any configuration. This is due to the increased fuel to air mixing and the quality of the atomization of the Full Config. The reaction zone for the w/o Hub configuration appears to be more extended in the axial direction. This is to a degree that it extends beyond the 160 mm-long flame tube. Due to the more volumetric flame propagation, the intensity of these flames appears to be reduced. Compared to the full configuration flames, the w/o Prefilmer flames have a less intense OH*. However, they are slightly more stretched in the axial direction. This is because larger fuel drops enter the reaction zone and take longer to evaporate.

The expected long reaction zones for both the w/o Swirler and Air Nozzle Only configurations are shown in the lower right of the image matrix. Note that due to the reduced flame operating range, these flames were operated at $T_{ad}$ = 2350 K. It appears that the w/o Swirler flame lifts more than the Air Nozzle Only configuration. This can be attributed to the better fuel vaporization of the Air Nozzle Only. Apparently, the heavier and more thermally conductive combustor casing (see Figure 4) results in more intensive heat transfer between the larger inner wall surfaces and the accumulated fuel film. The installation of the prefilmer only makes sense if the swirler is installed.

The operating range of the configurations is shown in Figure 16 as a function of jet velocity at $\Delta T$ = -100 K (spray injection). The $T_{air}$ at which the LBO limits were recorded are color-coded: blue symbols for $T_{air}$ = 155°C, gray symbols for 205°C, and red symbols for 255°C. A wider range of flame stability is indicated by a lower $T_{ad}$ LBO. This suggests that the flame was able to continue operating at lower temperatures.

For the Full Config, w/o Hub and w/o Prefilmer, the range of bulk velocities where LBO limits occurred was 91–140 m/s. The w/o Prefilmer had the largest operating range, consistently having a lower $T_{ad}$ LBO at $T_{air}$ = 155°C. Among other reasons, such as flow field changes, the authors assume the formation of larger fuel droplets at lower air temperatures was the primary reason the w/o prefilmer had a higher LBO margin. This may be due to "envelope" flames that formed around the larger droplets and burned in a diffusion mode at high temperatures. These hot burning fuel droplets provided the necessary radicals needed to maintain the chain reactions in the reaction zone. As $T_{air}$ increased, the fuel droplet sizes of the w/o Prefilmer approached those of the full configuration, which roughly equalized their LBO limits.

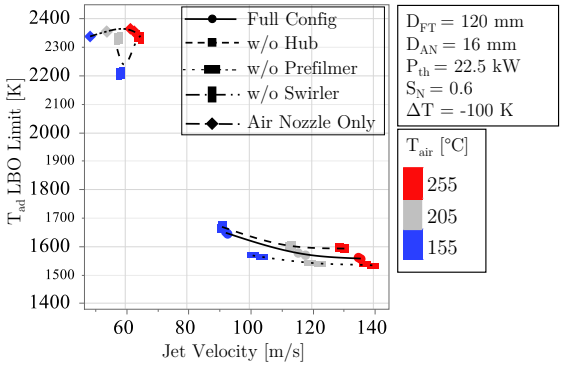


**FIGURE 16: LBO LIMIT PLOT FOR DIFFERENT COMBUSTOR CONFIGURATIONS**

Due to their reduced fuel evaporation even at higher air temperatures, the w/o Swirler (E) and Air Nozzle Only (F) configurations, showed a very narrow operating range of $T_{ad}$ LBO limit at > 2200 K. Since the swirling motion produced by the swirler is also absent, the turbulence and recirculation zone required for stable combustion and flame reignition in the flame tube are not established. The slightly lower $T_{ad}$ LBO value of the w/o Swirler configuration at $T_{air}$ = 155°C disappears as $T_{air}$ increases to 205–255°C. This is an indication of the larger fuel droplets burning at near-stoichiometric condition required to maintain the flame are no longer present as the air temperature increases.

Figure 17 shows the effect of increasing fuel ΔT on $NO_x$ emissions at various $T_{ad}$ for Full Config, w/o Hub, and w/o Prefilmer combustor configurations. $NO_x$ emissions increase with increasing $T_{ad}$ for all configurations and ΔT levels. This can be attributed to the higher flame temperature and the consequent higher thermal NO formation rates. For all fuel preheat levels ΔT, the Full Config consistently shows higher $NO_x$ levels (maximum difference: 4.5 ppm) than the other configurations. The main reason for this is that the reaction zones of the Full Config are more compact heat release zone (see Figure 15), as a result of better fuel-air mixing and fuel evaporation. This leads to higher local temperatures and increased thermal NO formation rate. The reason the Full Config operating points are not the same at the fuel-leanest conditions is an error in the execution of the experiment. This was due to a lower airflow setting which resulted in a higher $T_{ad}$ than desired. However, during data analysis, the correct $T_{ad}$ values were calculated and are plotted.

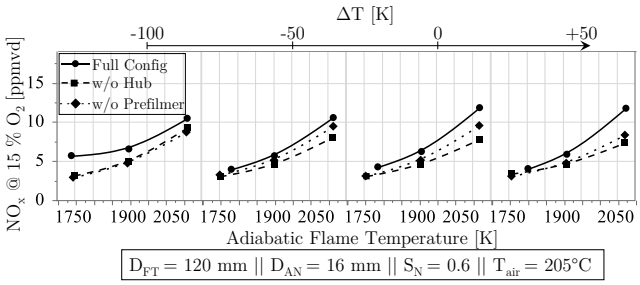


**FIGURE 17: $NO_x$ PLOTS FOR VARIOUS ΔT LEVELS AND COMBUSTOR CONFIGURATIONS**

$NO_x$ emission levels for all configurations appear to be largely independent of fuel temperature (ΔT) and spray regime, with a slight change in $NO_x$ levels as ΔT is increased above -50 K at $T_{ad}$ > 2000 K. At the fuel-leanest point ($T_{ad} \approx$ 1750 K) of Full Config, by increasing ΔT from -100 to -50 K, $NO_x$ levels decrease from 5.7 to 4 ppm due to improved fuel droplet size. For ΔT from -50 to 0 K and at $T_{ad}$ = 2050 K, the Full Config $NO_x$ increases by a minimum of 1.3 ppm from 10.6 to 11.9 ppm and remains constant up to ΔT = +50 K.

For the w/o Prefilmer configuration, increasing ΔT from -50 to +50 K results in a 1.1 ppm decrease in $NO_x$ from 9.5 to 8.4 ppm at $T_{ad}$ = 2050 K. A more propagated reaction zone for the w/o Hub and w/o Prefilmer configurations may play a role in the reduced $NO_x$ levels (see the OH* images in Figure 15). The $NO_x$ levels are very low for all configurations over the entire tested range. For an increase of $T_{ad}$ = 300 K, the $NO_x$ values approximately double in value, e.g. from 5.7 to 10.5 ppm, but do not show an extreme increase. Therefore, since the $NO_x$ emissions do not vary significantly, they do not play a major role in the evaluation of the configurations.

The configurations appear to have a significant effect on CO emissions, although the change in $NO_x$ levels was minimal. This is illustrated in Figure 18. The gradient of the increase in CO with decreasing $T_{ad}$ can be clearly seen. The w/o Hub flames emit the highest levels of CO for the entire range of $T_{ad}$ and for all ΔT levels. The CO levels are highest (81 ppm) due to the larger droplets formed by the injector and the reduced fuel evaporation at lower fuel temperatures (ΔT = -100 K) and leaner fuel-air mixture ($T_{ad}$ = 1750 K).

The CO values for w/o Prefilmer at $T_{ad} \geq$ 1900 K appear to be quite similar to the full configuration at all ΔT levels. However, at the leanest flame conditions ($T_{ad}$ = 1750 K), the w/o Prefilmer configuration shows consistently higher CO values, for example, by a maximum margin of 15 ppm at ΔT = +50 K. Inadequate oxidation of CO to $CO_2$ is caused by increased evaporation time due to larger fuel droplets. Note that the prefilmer increases the bulk velocity within the mixing channel and thus enhances secondary fuel atomization via air-blast effect. While the w/o Prefilmer CO levels decrease to almost the same level at ΔT = -50 K, it increases again to as high as 22 ppm at ΔT = +50 K and $T_{ad}$ = 1750 K. The decrease in CO at ΔT = -50 K is due to reduced fuel droplet size at spraying conditions.

The rapid expansion of evaporating fuel after superheated injection and subsequent deterioration of fuel-air mixing causes the increase in CO at ΔT = +50 K. The Full Config does not have this sharp increase in CO. A likely reason is that the higher velocity in the mixing channel caused by the prefilmer has improved fuel-air mixing downstream of the swirler.

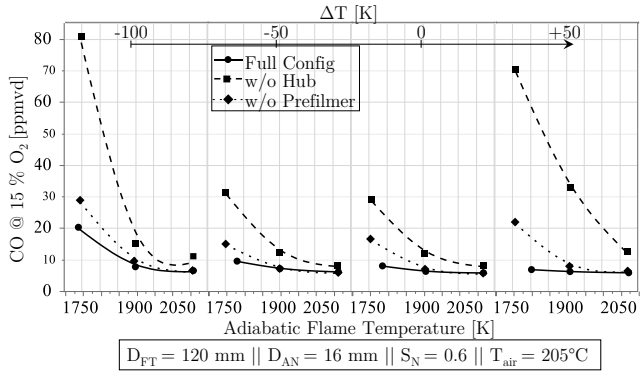


**FIGURE 18: CO PLOTS FOR VARIOUS ΔT LEVELS AND COMBUSTOR CONFIGURATIONS**

At ΔT = +50 K and $T_{ad}$ = 1750 K The w/o Hub, on the other hand, shows a significantly higher CO of 70.4 ppm compared to the w/o Prefilmer and Full Config at 22 and 7 ppm, respectively, due to its inability to block most of the expanding superheated fuel. It appears that due to the lower fuel-air mixing at the superheated conditions, the swirler hub had a significant effect on the CO levels. However, for the Full Config, as the fuel temperature increases (ΔT ≥ -50 K), the effect of the fuel temperature on the CO levels decreases. This is due to better mixing of the fuel with the air and blocking of the rapidly expanding fuel during superheated injection.

Figure 19 shows the effect of varying configurations on the flame HAB at different ΔT. Essentially, the reactivity of the mixture should be increased by increasing the fuel vaporization rate and improving the fuel-air mixture. This effect is expected to lead the flame stabilizing closer to the combustor head, resulting in lower flame HAB. As shown in Figure 11 *A*, an increase in air temperature from 155 to 255°C at ΔT = -100 K resulted in a minimal decrease in the HAB of 5 mm due to the evaporation of the fuel.

Nevertheless, Figure 19 shows the successive increase in HAB as ΔT increases for all configurations, but at different rates. The Full Config's improved mixing and ability to block most of the expanding fuel as ΔT increases from -100 to +50 K is reflected in its lowest value of HAB 9.5 mm at $T_{ad}$ = 1900 K among all configurations. This is significantly less than w/o Prefilmer and w/o Hub configurations whose HAB increases by 14 and 46.4 mm, respectively, for the same ΔT increase. It also helps to increase the velocity, which helps to improve the mixing of the fuel and air.

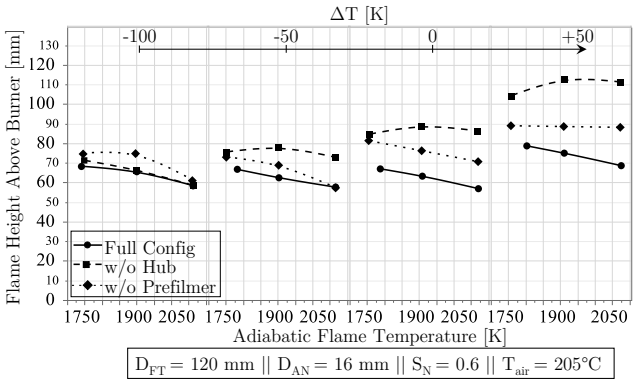


**FIGURE 19: HAB PLOTS FOR VARIOUS ΔT LEVELS AND COMBUSTOR CONFIGURATIONS**

Flame length data for the tested configurations as a function of ΔT and $T_{ad}$ are shown in Figure 20. It should be noted that in both the w/o Hub (C) and w/o Prefilmer (D) configurations, the reaction zones were so long that their upper ends were outside the cylindrical flame tube, which resulted in inaccurate FL calculation at all ΔT levels and $T_{ad}$ = 1750 K.

Better fuel-air mixing, improved fuel droplet evaporation, and lower axial velocity are generally responsible for lowering the flame lengths. Flame length values decrease as flame temperature increases. Under fuel-richer conditions, a more reactive mixture and higher fuel evaporation rate in the reaction zone results in shorter flames. As ΔT increases, FL decreases because the initial fuel droplet evaporation time decreases. This causes the reaction zone to be shortened. At all levels of ΔT, the full configuration is consistently shown to have the lowest FL values. The highest FL values for all configurations occur at the leanest fuel conditions, where velocity is highest and heat release rate is lowest.

The FL of the w/o Hub configuration decreases steadily as ΔT increases from -100 to 0 K, by 14.6 mm at $T_{ad}$ = 1900 K. Once the fuel is injected in the superheated condition (ΔT = +50 K), its FL value decreases by 20 mm compared to ΔT = 0 K. The continuous passage of the superheated fuel expanding through the hub caused more rapid oxidation of the fuel, which shortened the reaction zone.

The consistently higher FL values of the w/o Prefilmer than the Full Config at all ΔT levels are due to the difference in fuel-air mixing quality of the configurations. The flames at ΔT = - 50 K differs in size and intensity for both configurations as shown in Figure 15. The larger fuel droplets and longer evaporating time lead to longer reaction zones. At ΔT = 0 K, the FL gap between the Full Config and the w/o Hub configuration continues to increase with increasing $T_{ad}$. This is due to the improved fuel-air mixing as a result of the smaller fuel droplets in the Full Config.

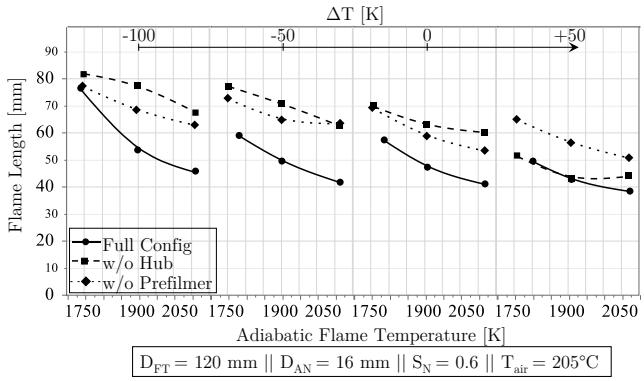


**FIGURE 20: FL PLOTS FOR VARIOUS ΔT LEVELS AND COMBUSTOR CONFIGURATIONS**

## 7. CONCLUSION

In the current research, a detailed experimental analysis of the newly developed swirl-assisted jet-stabilized combustor based on the lean premix prevaporize (LPP) concept was carried out at atmospheric pressure.The effect of different designs on emissions and flame characteristics was investigated by varying the injector type: pressure-swirl and plain-orifice. Preliminary non-reactive Mie scattering measurements revealed a significant fuel injection behavior difference. While the pressure swirl injector formed fine fuel droplets, the plain-orifice injector formed a straight fuel jet. The pressure-swirl and plain-orifice injectors also differed in the transition temperature from the spray to the superheated injection regime at $T_{fuel} = 210$ and 250°C, respectively. The $NO_x$ levels at $T_{ad} = 2050$ K for the plain-orifice in the sprayed condition were 6.5 ppm above the pressure-swirl levels. This difference was reduced to 1.5 ppm at the fuel saturation temperature ΔT = 0 K. This is an indication of the independence of the $NO_x$ levels from the primary atomization quality of the fuel for the analyzed combustor.

Mie scattering was used in reactive tests in order to investigate the degree of fuel evaporation prior to the reaction zone, where two operating parameters were varied. The fuel temperature was increased (ΔT = -100 to +50 K) at different air temperatures ($T_{air} = 155$ to 255°C). Independent observations were made of the effect of fuel and air temperature on fuel evaporation in the flame tube. The results showed that although the fuel temperature exceeded its saturation temperature by 50 K at the lowest air temperature ($T_{air} = 155$°C), liquid fuel plume was observed at the combustor head due to fuel re-condensation. The $NO_x$ and CO emissions were not affected by the variation of $T_{air}$. However, due to the degraded fuel-air mixture quality, the increase in ΔT resulted in a slight increase in $NO_x$. With superheated injection (ΔT = +50 K), the flame HAB increased by ≈ 15 mm compared to ΔT = 0 K. This was affected by rapid axial expansion of the superheated fuel and thus reduced fuel-air mixedness. This resulted in decreased reactivity of the fuel-air mixture entering the reaction zone.

The full and four modified configurations of the combustor were tested in terms of their influence on fuel evaporation, emissions, flame operating range and heat release zone shape. It was shown that with the investigated swirl-assisted jet-stabilized combustor concept, very low $NO_x$ and CO emissions with very compact flames can be achieved for the Jet A-1 combustion. Within the scope of the investigation, it was possible to show which components of the combustor have which share in the vaporization and mixing process.

Through the swirler hub enabled lower CO emissions at all ΔT levels by blocking large fuel droplets from entering the reaction zone. In addition to blocking the air bypassing the swirler in the mixing channel, the prefilmer increased the fuel-air velocity in the mixing channel. This led to improved fuel evaporation and CO values. The $NO_x$ levels of the full configuration were slightly higher than the w/o Hub and w/o Prefilmer configurations. This was because of the more compact reaction zones of the Full-Config, resulting in higher local temperatures. The flame operating range of the full configuration was similar to that of the w/o Hub and w/o Prefilmer configurations. However, the HAB and FL values of the Full Config were much lower than the w/o Hub and w/o Prefilmer. This was probably due to improved formation of the inner and outer recirculation zones. The operating ranges were very narrow for the w/o Swirler and Air Nozzle Only configurations due to the absence of the swirler, which made a significant contribution to the flame stabilization.

It can be concluded that the incorporation of the prefilmer, swirler and its hub results in improved performance of the combustor due to consistently and substantially lower CO, HAB and FL values of the Full Config at all fuel level of preheat. The above benefits compensate for the slightly reduced operating range and slightly higher $NO_x$ values of the Full Config.

## ACKNOWLEDGMENT

The efforts of Stefan Fiedler and Timo Wagner are greatly appreciated for their support throughout the testing campaign. Special thanks to the VT-DLR workshop, Jens Kreeb, Ralph Bruhn, Sven Schober and Michael Gröninger for their efforts in manufacturing the combustor. This research is funded by the German Aerospace Center (DLR) as an internal project.

## 8. REFERENCES

[1] Lee D. S., Fahey D. W., Skowron A., Allen M. R., and Burkhardt U., 2021,"The contribution of global aviation to anthropogenic climate forcing for 2000 to 2018," Atmospheric environment (Oxford, England 1994), **244**, p. 117834.

[2] Liu Y., Sun X., Sethi V., Nalianda D., Li Y.-G., and Wang L., 2017,"Review of modern low emissions combustion technologies for aero gas turbine engines," Progress in Aerospace Sciences, **94**, pp. 12–45.

[3] Lefebvre A. H., 1995,"The Role of Fuel Preparation in Low-Emission Combustion," Journal of Engineering for Gas Turbines and Power, **117**(4), pp. 617–654.

[4] Rokke P. E., and Hustad J. E., 2005,"Exhaust gas recirculation in gas turbines for reduction of CO2 emissions; combustion testing with focus on stability and emissions," International Journal of Thermodynamics, **8**(5), 167–173.

[5] Lefebvre A. H., and Ballal D. R., 2010. *Gas Turbine Combustion*, CRC Press: Taylor & Francis Group, Boca Raton, FL.

[6] Nickolaus D., Crocker D., Black D., and Smith C., 2002,"Development of a Lean Direct Fuel Injector for Low Emission Aero Gas Turbines," American Society of Mechanical

Engineers, International Gas Turbine Institute, Turbo Expo (Publication) IGTI, **1**.
[7] Behrendt T., Heinze J., and Hassa C., Eds., 2003. *Experimental Investigation of a New LPP Injector Concept for Aero Engines at Elevated Pressures*.
[8] Lammel O., Stöhr M., Kutne P., Dem C., Meier W., and Aigner M., 2012,"Experimental Analysis of Confined Jet Flames by Laser Measurement Techniques," J. Eng. Gas Turbines Power, **134**(4), 041506–041506-9.
[9] Izadi S., Zanger J., Baggio M., Seliger-Ost H., Kutne P., and Aigner M., 2024,"Experimental Investigation of the Effect of Superheated Liquid Fuel Injection On the Combustion Characteristics of Lean Premixed Flames," ASME. J. Eng. Gas Turbines Power(146), pp. 1–13.
[10] Kathrotia T., Oßwald P., Zinsmeister J., Methling T., and Köhler M., 2021,"Combustion kinetics of alternative jet fuels, Part-III: Fuel modeling and surrogate strategy," Fuel, **302**, p. 120737.
[11] Guillaume Vignat, Daniel Durox, and Sébastien Candel, 2022,"The suitability of different swirl number definitions for describing swirl flows: Accurate, common and (over-) simplified formulations," Progress in Energy and Combustion Science, **89**, p. 100969.
[12] Izadi S., Zanger J., Kislat O., Enderle B., Grimm F., Kutne P., and Aigner M., 2021,"Experimental Investigation of the Combustion Behavior of Single-Nozzle Liquid-FLOX®-Based Burners on an Atmospheric Test Rig," 0742-4795, **143**(7).
[13] Izadi S., Zanger J., Kislat O., Enderle B., Grimm F., Kutne P., Aigner M., and Kraus C., 2021,"A Design of Experiments Based Investigation of the Influence of Hot Cross-Flow Gas on a FLOX®-Based Single-Nozzle Liquid Burner," American Society of Mechanical Engineers, International Gas Turbine Institute et al. 2021 – Proceedings of the ASME Turbo(GT2021-59029).
[14] Saeed Izadi, 2018. *Characterization of Pressure Atomizers for a Single Nozzle Liquid FLOX® Burner Using Optical and Laser Diagnostics: Master Thesis*, Institute of Combustion Technology for Aerospace Engineering (IVLR), University of Stuttgart.
[15] Albregtsen F., 2008,"Reflection, refraction, diffraction, and scattering," University of Oslo: Oslo, Norway.
[16] Leo M. de, Saveliev A., Kennedy L. A., and Zelepouga S. A., 2007,"OH and CH luminescence in opposed flow methane oxy-flames," Combustion and Flame, **149**(4), pp. 435–447.
[17] Kathrotia T., 2011,"Reaction Kinetics Modeling of OH(∗), CH(∗), and C2(∗) Chemiluminescence," Heidelberg, Ruprecht-Karls-Universität.
[18] Zanger J., 2016,"Experimentelle Charakterisierung eines atmosphärisch betriebenen, jet-stabilisierten Mikrogasturbinenbrenners für Erdgas," Stuttgart, Universität.
[19] Bower H. E., Schwärzle A., Grimm F., Zornek T., and Kutne P., 2019,"Experimental Analysis of a Micro Gas Turbine Combustor Optimized for Flexible Operation with Various Gaseous Fuel Compositions," Journal of Engineering for Gas Turbines and Power, **142**(031015), pp. 1–9.
[20] Rachner M., 1998. *Die Stoffeigenschaften von Kerosin Jet A-1*, DLR, Abt. Unternehmensorganisation und -information.